INORGANIC CHEMISTRY

FRONTIERS

Accepted Manuscript

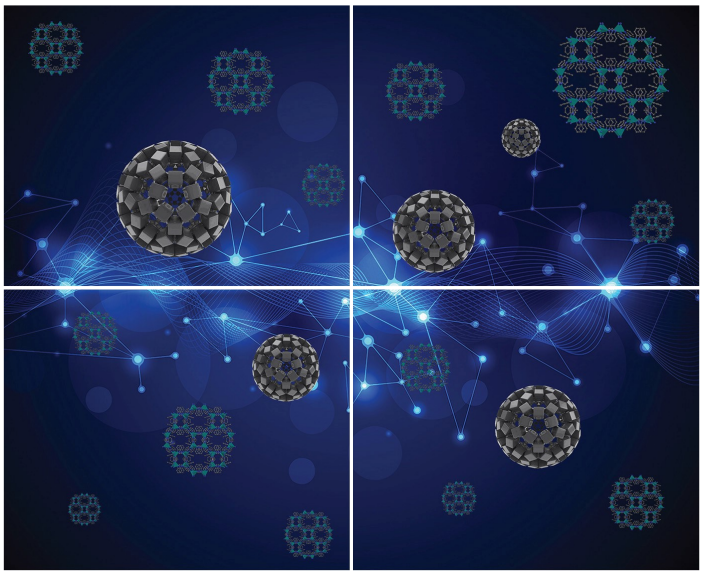

This article can be cited before page numbers have been issued, to do this please use: N. Sato, K. Toki, T. Tateishi, M. Tsumura, R. Toyoda, S. Takaishi, Y. Kurashige, K. Sugimoto and R. Sakamoto, *Inorg. Chem. Front.*, 2026, DOI: 10.1039/D6QI00339G.

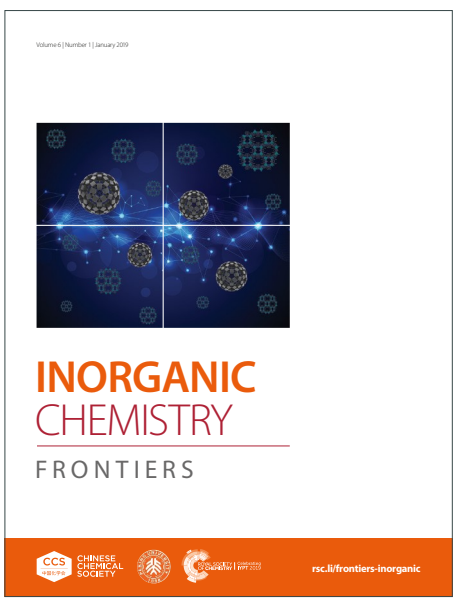

View Article Online
DOI: 10.1039/D6QI00339G

ARTICLE

Nickel(II) porphyrin/fullerene C_{70} porous molecular cocrystal featuring a robust one-dimensional channel

Received 00th January 20xx,
Accepted 00th January 20xx

DOI: 10.1039/x0xx00000x

Nobuhiro Sato,[a] Kosuke Toki,[a] Tomoki Tateishi,[a,b] Masaya Tsumura,[c] Ryojun Toyoda,[a] Shinya Takaishi,[a] Yuki Kurashige,[c] Kunihisa Sugimoto,[d] and Ryota Sakamoto*[a,e]

Molecular cocrystals are crystalline materials composed of multiple types of molecular components held together by noncovalent interactions. Among these, porphyrin-fullerene cocrystals represent a well-studied class of supramolecular assemblies. The close packing arrangement between porphyrins and fullerenes is known to contribute to high crystallinity and structural stability. Porphyrin-fullerene cocrystal systems including C_{60}, which has a spherical shape, have provided insights on intermolecular interaction. In contrast, cocrystals incorporating C_{70}, which has an ellipsoidal shape, remain relatively unexplored, and the influence of fullerene shape on cocrystal structures and stability remains unclear. In this study, we investigate the differences between C_{60} and C_{70} using cocrystals of a nickel(II) porphyrin derivative (**NiTEPP**) with these fullerenes. Two distinct cocrystals were successfully obtained: the porous cocrystal **NiTEPP/C_{70}** featuring one-dimensional channels, and the nonporous crystal **NiTEPP/C_{70}-n**. High-pressure single-crystal X-ray diffraction results show that these cocrystals maintained their single crystal structure under high pressure. Furthermore, intermolecular interaction energies depending on the fullerene species were evaluated using density functional theory calculations. The combined experimental and theoretical results demonstrate that the shape of the fullerene plays a crucial role in governing intermolecular interactions and structural stability, and these results provide valuable guidelines for the rational design of molecular cocrystals with controlled intermolecular interactions.

Introduction

Molecular cocrystals formed by the self-assembly of multiple molecular components has attracted increasing attention in recent years.[1–3] By precise controlling intermolecular interactions[4] and molecular geometries,[5] it is possible to enhance the molecular ordering[6] and structural stability.[7] Cocrystallization enables the realization of structures and packing motifs that are not accessible in conventional unimolecular crystals,[8,9] thereby expanding the scope of crystal engineering based on the inherent flexibility and diversity of molecules.[10–12] Furthermore, studies on molecular cocrystals play a crucial role in understanding of intermolecular interactions[13–15] The elucidation of the principles governing precise molecular arrangements is expected to facilitate the design of molecular assemblies and future applications in functional materials.[16–19]

Among molecular cocrystals, porphyrin–fullerene systems have emerged as a well-studied class of supramolecular assemblies.[20–22] In these cocrystals, porphyrin molecules are regularly arranged around fullerene molecules, and intermolecular interactions—π–π stacking interactions and van der Waals forces—are known to contribute significantly to stabilize the crystal structure.[23-25] The close contact of fullerene molecules with the porphyrin planes[26,27] results in characteristic molecular packing, thereby improving the crystallinity and stability of the cocrystals.[24] To date, numerous porphyrin–fullerene cocrystals based predominantly on spherical C_{60} have been reported.[27–31] These results provide important insights into the structural features and design principles of molecular crystals. In contrast, reports on molecular cocrystals incorporating ellipsoidal C_{70} are relatively limited compared with those involving C_{60}.[32–34] Consequently, systematic investigations into the differences in intermolecular interactions between porphyrins and different fullerene species, such as C_{60} and C_{70}, as well as their impact on cocrystal structures and stability, remain scarce.[35] Correspondingly, cocrystal systems involving metalloporphyrin derivatives in which both C_{60} and C_{70} afford the same crystal system remain limited.[36,37]

In this situation, we previously prepared a cocrystal composed of a Ni-porphyrin derivative **NiTEPP**[38,39] (Figure 1a) and C_{60} (hereafter **NiTEPP/C_{60}**).[40] The structure of **NiTEPP/C_{60}** was characterized and analyzed by single-crystal X-ray diffraction (scXRD) measurement. This measurement revealed that porphyrin molecules regularly encapsulate C_{60}, forming two-dimensional honeycomb networks, in which three porphyrin molecules surround a single C_{60} molecule. These honeycomb layers stack along the *c* axis in AA* stacking mode. Owing to the stacking manner of the layers and the molecular ordering, permanent one-dimensional channels were confirmed to exist in the crystal lattice. These structural features lead to the formation of a crystal with the $P\bar{3}c1$ space group. The presence of

[a] Department of Chemistry, Graduate School of Science, Tohoku University, 6-3 Aramaki Aza-Aoba, Aoba-ku, Sendai 980-8578, Japan.
[b] Frontier Research Institute for Interdisciplinary Sciences (FRIS), Tohoku University Aramaki aza Aoba 6-3, Aoba-ku, Sendai 980-8578, Japan.
[c] Department of Chemistry, Graduate School of Science, Kyoto University, Kitashirakawa Oiwake-cho, Sakyo-ku, Kyoto, Japan.
[d] Department of Chemistry, Kindai University, 3-4-1 Kowakae, Higashi-Osaka, Osaka 577-8502, Japan.
[e] Division for the Establishment of Frontier Sciences of Organization for Advanced Studies at Tohoku University, 2-1-1 Katahira, Aoba-ku, Sendai 980-8577, Japan.

View Article Online
DOI: 10.1039/D6QI00339G

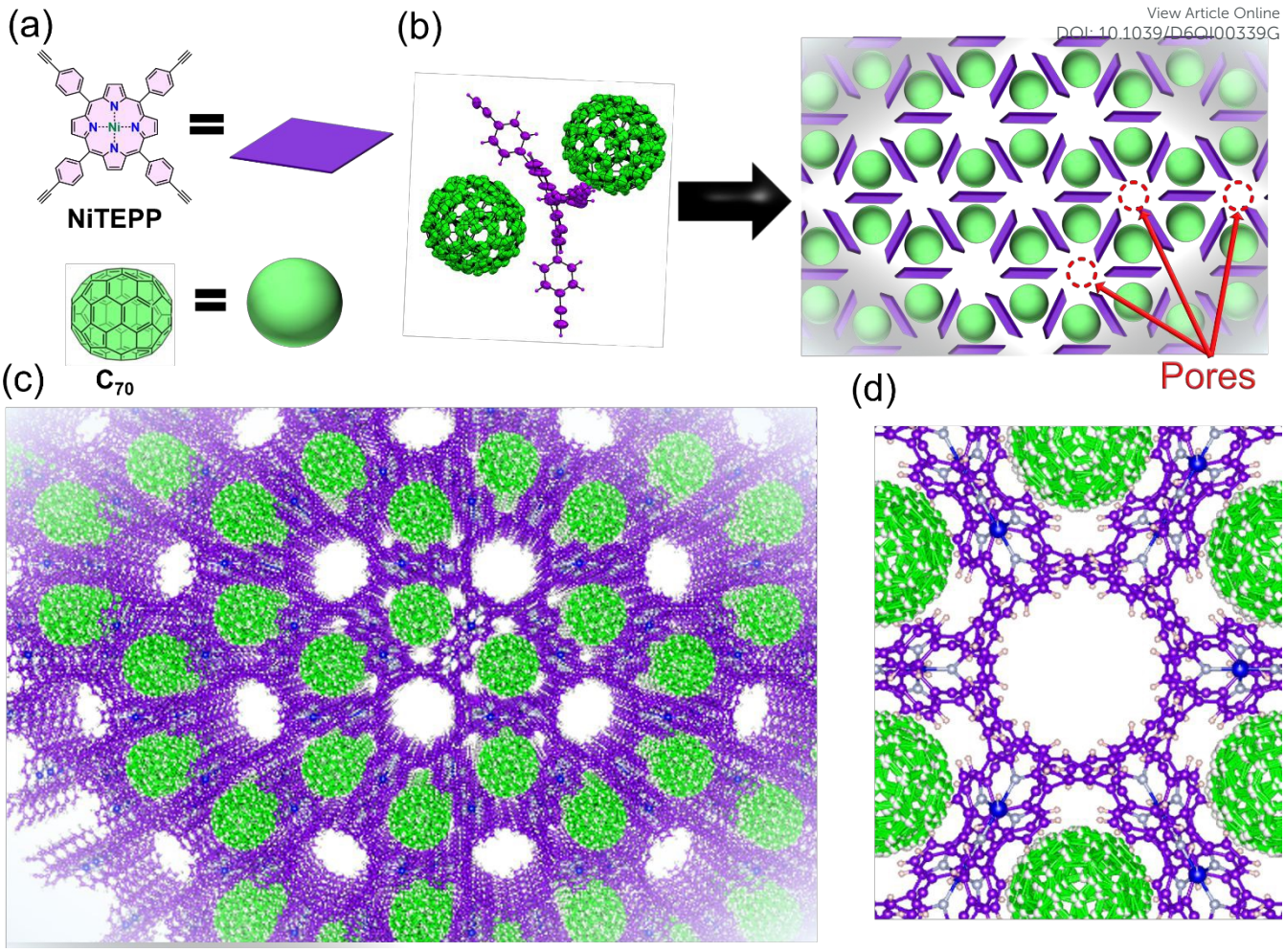

Figure 1. Schematic illustration of the single-crystal structure of porous NiTEPP/C_{70} cocrystal. (a) Molecular structures of **NiTEPP** and C_{70}. **NiTEPP** and C_{70} are shown in purple and green, respecitively. (b) Schematic illustration of the interaction between **NiTEPP** and C_{70} and the resulting honeycomb 2D network. (measured at 120 K; thermal ellipsoids are drawn at the 50% probability level). (c) Stereoscopic crystal structure of **NiTEPP/C_{70}** viewed along the c-axis. (d). scXRD structure of **NiTEPP/C_{70}** viewed along the c-axis displaying Q peaks with intensities of more than 0.5 e/Å^3 were set to be shown, while no significant residual electron density is observed in the channel.

the two-dimensional honeycomb structure with intrinsic voids, together with its remarkable stability under acidic and basic conditions as well as external pressure, is rare among molecular crystals and represents a highly unique structural feature.[41] Furthermore, reversible adsorption and desorption behavior toward solvents and gases demonstrates the functional utility of the one-dimensional channel in the crystal.

In this study, we report the preparation of two types of cocrystals composed of **NiTEPP** and C_{70}. These structures were thoroughly characterized by scXRD measurements. One cocrystal, **NiTEPP/C_{70}**, is isostructural with **NiTEPP/C_{60}**. In **NiTEPP/C_{70}**, C_{70} molecules occupy both axial positions of Ni center in **NiTEPP**. The porphyrin-to-fullerene ratio is determined to be 3:2 in **NiTEPP/C_{70}**. The other one is **NiTEPP/C_{70}-n** which has no void. In **NiTEPP/C_{70}-n**, only one axial position is occupied by a **NiTEPP** molecule, leading to a different ratio of **NiTEPP** and fullerene molecules, 1:1, in **NiTEPP/C_{70}-n**. DFT calculation revealed that **NiTEPP/C_{70}** exhibits a higher interaction energy than its C_{60} analogue, which is likely to be attributed to the elongated molecular shape of C_{70}. In contrast, **NiTEPP/C_{70}-n** shows a lower interaction energy compared to **NiTEPP/C_{70}**. These results demonstrate the effect of C_{70} incorporation instead of C_{60} on intermolecular interactions in the cocrystal with **NiTEPP**.

Results and discussion

NiTEPP was synthesized according to the previously reported procedure, and cocrystallization of **NiTEPP** with C_{70} was attempted using crystallization conditions analogous to those employed for **NiTEPP/C_{60}**.[40] However, the cocrystallization was unsuccessful using the liquid-liquid diffusion method. After optimization of the crystallization conditions, a vapor diffusion method (Figure S1), using a 1:1 (v/v) mixture of $CHCl_3$ and CS_2 as the good solvent and hexane as the poor solvent, afforded black rod-shaped crystals of **NiTEPP/C_{70}** deposited on the inner wall of the vial.

The structure of **NiTEPP/C_{70}** was characterized by scXRD measurement (Figures 1 and S2 and Table S1). Unlike the previously reported **NiTEPP/C_{60}** cocrystal, C_{70} molecule does not possess a threefold rotational symmetry. The assignment of C_{70} molecules in

View Article Online
DOI: 10.1039/D6QI00339G

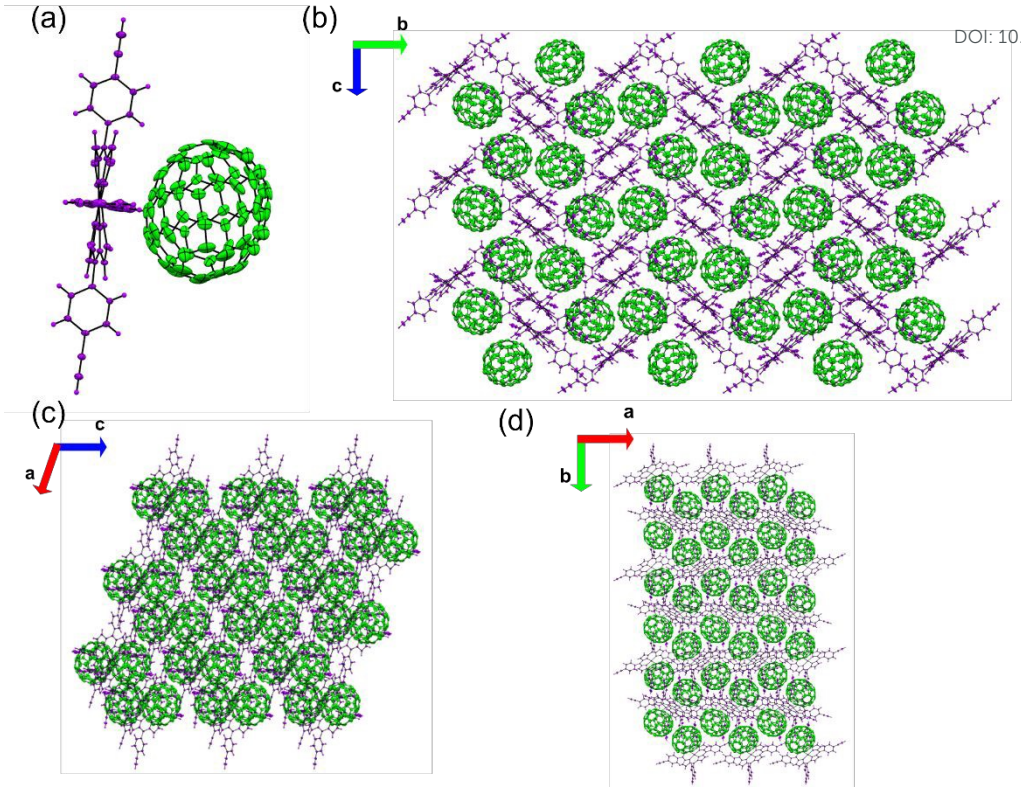

Figure 2. Schematic illustration of the single-crystal structure of nonporous NiTEPP/C_{70}-n cocrystal. (a) ORTEP drawing of **NiTEPP/C_{70}-n**, showing that the Ni(II)porphyrin plane does not bend along with C_{70}. (b) Crystal packing structure of **NiTEPP/C_{70}-n** viewed along *a* axis. (c) Crystal packing structure of **NiTEPP/C_{70}-n** viewed along *b* axis. (d) Crystal packing structure of **NiTEPP/C_{70}-n** viewed along *c* axis.

NiTEPP/C_{70} required a disorder treatment that a single C_{70} molecule was modelled over three symmetry equivalent orientations because the $P\bar{3}c1$ possesses a threefold rotational axis throughout the crystal (Figure S3). The crystal system of **NiTEPP/C_{70}** is formed by the arrangement of C_{70} molecules along both axial positions of **NiTEPP**, similar to **NiTEPP/C_{60}** (Figure 1b). The interactions of three **NiTEPP** molecules surrounding a single C_{70} molecule give rise to a two-dimensional honeycomb network with a porphyrin-to-fullerene ratio of 3:2, extending along the *a* and *b* axes. This two-dimensional honeycomb network is stacked along the *c* axis in an eclipsed stacking mode, leading to the formation of one-dimensional channels running parallel to the *c* axis belonging to the space group $P\bar{3}c1$ with permanent voids (Figure 1c). For the system of **NiTEPP/C_{60}**, when the residual electron density (Q-peak) within the channels was below 0.5 e/Å³, simultaneous thermogravimetry-mass spectrometry measurements indicated that no solvent molecules were present in the voids. For **NiTEPP/C_{70}**, no Q-peaks greater than 0.5 e/Å³ were found in the channel. This result suggests that no solvent molecules are present in the voids. At 120 K, the unit-cell parameters of **NiTEPP/C_{70}** were determined to be *a* = 23.05 and *c* = 21.90 Å (Table S1). Compared with those of **NiTEPP/C_{60}** (*a* = 22.13 and *c* = 21.66 Å), these values correspond to expansions of 1.97% along the *a* axis and 2.85% along the *c* axis, respectively. The unit-cell volume of **NiTEPP/C_{70}**, 10080 Å³, corresponds to the expansion of 6.93% from **NiTEPP/C_{60}** (9188 Å³). In previously reported cocrystals of metalloporphyrin with C_{60} and C_{70} that afford same crystal system, the unit cell volumes change negligibly (within 1%).[36,37] In contrast, the present system represents a unique cocrystal in which the same crystal system is retained for both C_{60} and C_{70}, while exhibiting a pronounced change in unit cell volume of 6.9%. To evaluate the geometric relationship among fullerene molecules in detail, the angles and distances of the component molecules were analysed. All disorder-modelled C_{70} molecules, the long molecular axis is found to be tilted by 34.7° relative to the *c* axis (Figure S4). In the case of the shortest centroid–centroid distances between fullerenes, **NiTEPP/C_{60}** shows the distances of 13.29 Å along the two-dimensional network direction (Figure S5a)and 10.85 Å along the *c* axis (Figure S5b), respectively. In **NiTEPP/C_{70}**, the distances increase to 13.71 (Figure S5c)and 11.15 Å (Figure S5d), respectively. In addition, the distances between the Ni center of **NiTEPP** and the centroid of the fullerene molecule was evaluated in both **NiTEPP/C_{60}** and **NiTEPP/C_{70}**. At 120 K, the distances are determined to be 7.05 Å for **NiTEPP/C_{60}** and 7.19 Å for **NiTEPP/C_{70}**, respectively. Furthermore, based on a previous study,[42] the angle of Ni center of **NiTEPP** and two mutually opposing *meso*-carbon atoms in the porphyrin, defined as *α*, are also determined to be 161.4° for **NiTEPP/C_{60}** and 159.5° for **NiTEPP/C_{70}**, respectively. The anisotropic, elongated geometry of C_{70} hinders the Ni(II)porphyrin from adopting a fully surrounding configuration, in contrast to spherical C_{60}. The geometric differences in the crystal are attributed to the nonspherical shape of the C_{70} molecule, which possesses an intrinsic long axis and is larger than C_{60}.

Next, the void volume was evaluated using the void calculation function implemented in Mercury. A probe radius of 1.8 Å was applied, following the same conditions as those used for **NiTEPP/C_{60}**.

View Article Online
DOI: 10.1039/D6QI00339Q

At 120 K, the void volume of **NiTEPP/C_{60}** was determined to be 1190 Å^3 per unit-cell, whereas that of **NiTEPP/C_{70}** was 1260 Å^3. This value corresponds to an increase of 8.6% in **NiTEPP/C_{70}**. The calculated void fractions are 12.7% for **NiTEPP/C_{60}** (Figure S6) and 12.9% for **NiTEPP/C_{70}** (Figure S7). Furthermore, pore radius analysis (Figures S8 and S9) revealed that the minimum pore radius was 3.34 Å for **NiTEPP/C_{60}** and 3.71 Å for **NiTEPP/C_{70}**, respectively. These observations suggest that the fullerene geometry modulates both the void fraction and pore size in the isostructural crystal structure.

We note that for **NiTEPP/C_{70}**, scXRD analysis was successfully performed even at ambient temperature (293 K; Figure S10 and Table S2). The molecular arrangement of **NiTEPP** and C_{70} was determined to be same as the crystal strucure of **NiTEPP/C_{70}** measured at 120 K. Compared with C_{60}, C_{70} possesses lower molecular symmetry and is more susceptible to orientational disorder, which generally makes scXRD analysis challenging.[43,44] Consequently, only a limited number of crystal structures containing C_{70} have been successfully analyzed at ambient temperatures.[22,45] For **NiTEPP/C_{70}**, although an increase in the degree of disorder of the C_{70} molecules was observed at 293 K, the crystals satisfied the standard crystallographic quality criteria when the same disorder model as that applied at 120 K was applied. The successful single-crystal structure determination at ambient temperature is attributed to the fact that the orientation of the C_{70} molecules is partially restricted by interactions with the porphyrin planes,[46] and further constrained by the three-directional encapsulation of the C_{70} molecules by **NiTEPP**, which spatially confines the molecular position in the crystal lattice.

Furthermore, in the course of the recrystallization of **NiTEPP** and C_{70}, other single crystals with a morphology different from that of **NiTEPP/C_{70}** were found, which were subjected to scXRD (referred to **NiTEPP/C_{70}-n**; Figures 2 and S11 and Table S3). Structural analysis for **NiTEPP/C_{70}-n** revealed that the porphyrin and C_{70} molecules are closely arranged and that C_{70} is located on only one side of the **NiTEPP** axial position, unlike **NiTEPP/C_{70}**. An adjacent porphyrin molecule occupies the opposite side of the porphyrin axial position. As a result, **NiTEPP** and C_{70} form a 1:1 complex, and dense packing of this complex within the crystal leads to the formation of a nonporous structure (Figure 2). The asymmetric arrangement and nonporous structure of **NiTEPP/C_{70}-n** contrasts with that of **NiTEPP/C_{70}**. The distance between the Ni center of **NiTEPP** and the centroid of C_{70} molecule was evaluated in the same manner as for **NiTEPP/C_{70}**. In **NiTEPP/C_{70}-n**, this distance was determined to be 6.49 Å, which is quite shorter than those observed in the structures of **NiTEPP/C_{60}** and **NiTEPP/C_{70}**. The shortest Ni‑C distance between **NiTEPP** and C_{70} was determined to be 2.87 Å, which is shorter than typical π–π stacking distances.[22] This suggests that specific porphyrin–fullerene interactions contribute to the proximity between the two components. In addition, the angle α of **NiTEPP** in **NiTEPP/C_{70}-n** was measured using the same definition as mentioned above. Although two angles α can be defined for **NiTEPP/C_{70}-n** due to the inequivalence of the front and back sides of the porphyrin plane, the smaller value was adopted as a representative descriptor of the structural distortion. As a result, α was determined to be 175.9°, which is markedly larger than those of **NiTEPP/C_{60}** and **NiTEPP/C_{70}**. This indicates that **NiTEPP** in **NiTEPP/C_{70}-n** undergoes minimal curvature (Figure 2a). In contrast to **NiTEPP/C_{70}**, **NiTEPP/C_{70}-n** adopts an asymmetric and densely packed 1:1 architecture in which C_{70} is positioned on only one side of **NiTEPP**. The different spatial arrangement in **NiTEPP/C_{70}-n** leads to a nonporous structure with close intermolecular contact, even with the porphyrin–fullerene interactions stabilizing both the crystal structures of **NiTEPP/C_{70}** and **NiTEPP/C_{70}-n**.

Subsequently, the obtained crystals were subjected to a series of characterizations. Powder X-ray diffraction (PXRD) analysis (Figure S12) revealed that the sample prepared via Figure S1 contains **NiTEPP/C_{70}** and **NiTEPP/C_{70}-n** phases but is overall a multiphase mixture. Accordingly, all subsequent measurements were conducted using this mixture. To probe the solid-state interactions, spectroscopic analyses were performed. The IR spectrum (Figure S13) exhibits characteristic bands attributable to both **NiTEPP** and C_{70}, confirming the coexistence of these components. The solid-state UV–vis spectrum (Figure S14) shows a distinct shift in the bands assignable to **NiTEPP**, which is attributed to intermolecular interactions with C_{70} in the solid state. The direction of this shift is consistent with that observed in the previously reported **NiTEPP/C_{60}** system,[40] supporting a similar interaction mode. N_2 gas sorption measurements at 77 K were then carried out using the mixture sample. The sorption isotherm (Figure S15) exhibits Type I behavior, indicative of microporosity, and shows reversible adsorption–desorption, demonstrating stable uptake and release of N_2. From this N_2 sorption isotherm, a monolayer adsorption capacity (V_m) and Brunauer–Emmett–Teller (BET) surface area were estimated to be 49.2 cm^3(STP) g^{-1} and 214 m^2 g^{-1}, respectively. For comparison, theoretical values derived from the crystal structure are 60.9 cm^3(STP) g^{-1} and 265 m^2 g^{-1}, respectively. The smaller experimental values are attributed to the existence of nonporous **NiTEPP/C_{70}-n** crystals in the used solid sample, besides porous **NiTEPP/C_{70}** crystals, which reduces the overall adsorption capacity. The pore size distribution was further evaluated from the adsorption isotherm using the NLDFT–GCMC method. (Figure S16) The distribution exhibits a maximum at 0.847 nm, slightly larger compared to that of **NiTEPP/C_{60}**, and indicates a slight increase in pore size consistent with the expansion of the unit cell.

Next, DFT calculations were performed using the CP2K program[47] to evaluate the interactions between the **NiTEPP** framework and fullerene molecules. A dispersion correction was applied to account for van der Waals interactions (see SI for the computational details). The structures of **NiTEPP/C_{60}**, three types of disordered **NiTEPP/C_{70}**, and **NiTEPP/C_{70}-n** were geometrically optimized. The interaction

Table 1. Calculated interaction energies (ΔE) and dispersion contributions (ΔE_{disp}) per fullerene

	ΔE (kcal/mol)	ΔE_{disp} (kcal/mol)
NiTEPP/C_{60}	–94.98	–102.60
NiTEPP/C_{70} (Type 1)	–102.05	–111.78
NiTEPP/C_{70} (Type 2)	–102.05	–111.35
NiTEPP/C_{70} (Type 3)	–101.17	–112.06
NiTEPP/C_{70}-n	–88.47	–94.93

View Article Online
DOI: 10.1039/D6QI00339G

energies were then calculated as the difference between the energies of the total energy of the optimized cocrystal and the sum of the isolated **NiTEPP** framework and a single fullerene molecule. The interaction energies ΔE per fullerene molecule were calculated for these five optimized structures (Table 1). The interaction energy can be decomposed into four energetic components.[48] To clarify the nature of ΔE, we also evaluated the dispersion contribution ΔE_{disp} separately. Notably, the dispersion contribution accounts for most of the total interaction energy in all systems. Among the examined systems, **NiTEPP/C_{70}** exhibits significantly larger stabilization (ΔE = 101.76 kcal/mol, averaged over three symmetry related configurations) than **NiTEPP/C_{60}** (ΔE = 94.98 kcal/mol). This difference reflects the larger contact surface area between C_{70} and **NiTEPP** framework. Importantly, the magnitude of ΔE in these systems is considerably larger than values reported for conventional theoretical studies of supramolecular assemblies.[48,49] This result suggests that the three-directional encapsulation by **NiTEPP** effectively amplifies the stabilization based on the dispersion contribution through simultaneous multipoint interactions. The stronger stabilization of C_{70} relative to C_{60} is consistent with previous theoretical studies.[49,50] Conversely, **NiTEPP/C_{70}-n** exhibits a smaller interaction energy (ΔE = 88.47 kcal/mol) compared with the three-directionally surrounded **NiTEPP/C_{70}** cocrystal. Nevertheless, the magnitude of ΔE remains substantially large, even though in **NiTEPP/C_{70}-n** each C_{70} interacts with only a single **NiTEPP** unit. This significant stabilization can be attributed to the proximity between **NiTEPP** and C_{70} in **NiTEPP/C_{70}-n**, which enhances short-range dispersion interactions. The smaller overall interaction energy arises from the reduced number of **NiTEPP** units directly interacting with the C_{70} molecule. Consequently, the overall contact surface area is reduced in **NiTEPP/C_{70}-n**, leading to fewer dispersion interactions per fullerene molecule. Overall, these results indicate that dispersion interactions dominate the stabilization of the **NiTEPP**/fullerene cocrylstal structures and the strength of stabilization is determined by both the number of interacting **NiTEPP** units and their spatial arrangement around the fullerene molecules.

Finally, we investigated the pressure resistance of **NiTEPP/C_{70}** and **NiTEPP/C_{70}-n** in their single-crystalline states. High-pressure scXRD measurements were conducted following the same procedure previously reported for **NiTEPP/C_{60}**.[38] Single-crystalline samples were placed in a diamond anvil cell, and scXRD measurements were performed at 300 K with gradually increasing pressure in the anvil cell. Under the low pressure at 0.60 GPa, **NiTEPP/C_{70}** retained a quasi-trigonal crystal structure, and the unit-cell volume decreased monotonically with increasing pressure (Figure 3a–d and Table S4). With increased external pressure to 1.4 GPa, the indexing match rate of the observed diffraction peaks against the unit-cell dropped sharply (Figure 3b). This behaviour indicates that the crystal structure of **NiTEPP/C_{70}** collapses in this pressure range of 0.60 to 1.4 GPa. Notably, the collapse pressure is lower than that of **NiTEPP/C_{60}**, which retains its single crystal structure up to 2.2 GPa.[40] Still, the level of pressure resistance for **NiTEPP/C_{70}** remains relatively high even when compared with other porous organic crystals.[51,52] Analysis of the changes in the lattice parameters as a function of the applied

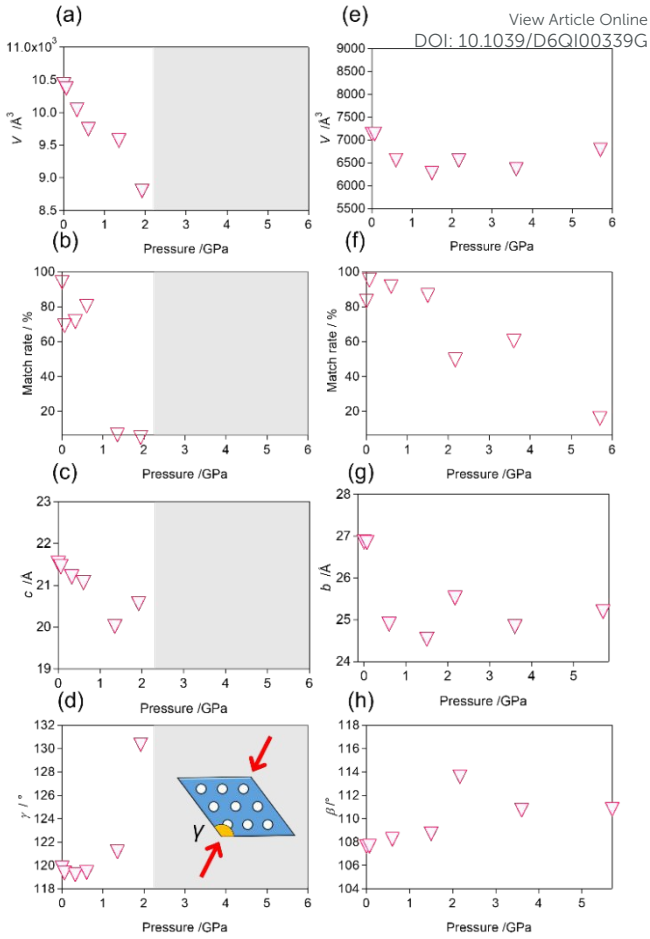

Figure 3. (a–d) Changes in the cell parameters as a function of applied pressure for **NiTEPP/C_{70}**. (a) The unit cell volume *V*. (b) The match rate of detected diffraction peaks to the indexed unit cell. (c) The *c* axis length. (d) The *γ* angle. (e–h) Changes in the cell parameters as a function of applied pressure for **NiTEPP/C_{70}-n**. (e) The unit cell volume *V*. (f) The match rate of detected diffraction peaks to the indexed unit cell. (g) The *b* axis length. (h) The *β* angle. The ranges of both the vertical and horizontal axes are unified for **NiTEPP/C_{70}** and **NiTEPP/C_{70}-n** for direct comparison. Note that pressures above 1.9 GPa were not measured for **NiTEPP/C_{70}**.

pressure revealed that, similar to **NiTEPP/C_{60}**, structural collapse in **NiTEPP/C_{70}** is accompanied by elongation along the *c* axis and an increase in the *γ* angle (Figure 3c, d). This deformation mode is consistent with the structural response expected when pressure is applied from the obtuse *γ* side of the rhombic unit-cell. The lower collapse pressure of **NiTEPP/C_{70}** is likely attributable to the anisotropic molecular shape of C_{70}. Although the overall crystal symmetry is described by space group $P\bar{3}c1$ in both **NiTEPP/C_{70}** and **NiTEPP/C_{60}**, local structural analysis indicates that the C_{70} molecules do not occupy crystallographically equivalent positions relative to the three surrounding **NiTEPP** units. Such microscopic structural distortions are therefore considered to facilitate pressure-induced structural collapse.

In the case of **NiTEPP/C_{70}-n**, the unit-cell volume was slightly decreased with increasing pressure, compared to **NiTEPP/C_{70}** (Table

S5 and Figure 3e). This difference in the decreased volume is likely because **NiTEPP/C_{70}-n** does not have any voids in its crystal structure. The limited compressible free volume is likely to be attributed for the smaller volume change against the applied pressure. When the pressure was increased from 3.6 to 5.7 GPa, the indexing match rate of the observed diffraction peaks against the unit-cell was significantly decreased (Figure 3f), accompanied by an anomalous increase in the detected unit-cell volume. Unlike **NiTEPP/C_{70}**, neither the *b* axis length nor the *β* angle, both of which exhibited relatively large variations, exhibited a systematic trend with increasing pressure (Figure 3g, h). These results indicate that **NiTEPP/C_{70}-n** has a relatively high-pressure resistivity of among nonporous molecular crystals.[53]

Conclusions

In this study, two types of the porphyrin-fullerene cocrystals were prepared from **NiTEPP** and C_{70}: porous **NiTEPP/C_{70}** cocrystal and nonporous **NiTEPP/C_{70}-n** cocrystal. Single-crystal X-ray diffraction analyses of **NiTEPP/C_{70}** and **NiTEPP/C_{70}-n** revealed the differences in the porphyrin-to-fullerene ratio and these packing arrangement. High-pressure scXRD measurements elucidated the pressure-dependent structural behaviors of both cocrystals and their structural robustness under high pressure. In addition, DFT calculations revealed that cocrystallization of **NiTEPP** with C_{70} provides greater stabilization than that with C_{60}. The detailed comparison of the intermolecular interactions in **NiTEPP/C_{60}** and **NiTEPP/C_{70}** revealed that the increasing the contact surface area between C_{70} and **NiTEPP** framework in **NiTEPP/C_{70}** critically increased the porphyrin-fullerene interactions. The insights gained in this study provide valuable a useful guidance for the design of crystalline architecture based on intermolecular interactions and are expected to contribute to advances in crystal engineering and related fields.

Author contributions

N.S.: conceptualization, data curation, investigation, formal analysis, writing original manuscripts, review, and editing. K.T.: investigation. T.T.: writing original manuscripts, review, and editing. M.T.: Calculation, writing computational section's manuscripts. R.T.: funding acquisition, methodology, resource, review, and editing. S.T.: methodology, resource. Y.K.: methodology on computational section, review, and editing. K.S.: high-pressure SXRD. R.S.: conceptualization, formal analysis, funding acquisition, methodology, project administration, resource, supervision, writing original manuscripts, review, and editing.

Conflicts of interest

There are no conflicts to declare.

Data availability

The data supporting this article have been included as part of the supplementary information (SI). Supplementary information: Synthetic procedure, Disorder process, X-ray crystallographic details, High pressure X-ray crystallographic details, and computational details. See DOI: xxxxxxxxxxxxx. CCDC 2527177–2527179 contain the supplementary crystallographic data for this paper.[54a-c]

Acknowledgements

This work was supported by JST-CREST (JPMJCR24S6 to R.S.) and JST-FOREST (JPMJFR203F to R.S. and JPMJFR221R to Y.K.). This work was also supported by MEXT/JSPS KAKENHI Grant Numbers JP25H01644, JP25H01999, JP25H02031, JP24K01494, JP22H05145, JP25KJ0562). We acknowledge the Asahi Glass Foundation (R.S.) for financial support. The computation was partly performed at the Research Center for Computational Science, Okazaki, Japan (Project: 25-IMS-C029). A part of SXRD measurements was performed at SPring-8 BL02B1 with the approval of the Japan Synchrotron Radiation Research Institute (JASRI) (Proposal No. 2025B1724).

Notes and reference

1 D. C. Sakhiya and C. H. Borkhataria, A review on advancement of cocrystallization approach and a brief on screening, formulation and characterization of the same, *Heliyon*, 2024, **10**, e29057.
2 J. Roshni and T. Karthick, A Comprehensive Review on Theoretical Screening Methods for Pharmaceutical Cocrystals, *J. Mol. Struct.*, 2025, **1321**, 139868.
3 S. Ren, G.-Y. Qiao and J.-R. Wu, Supramolecular-macrocycle-based functional organic cocrystals, *Chem. Soc. Rev.*, 2024, **53**, 10312–10334.
4 J. Alfuth, K. Kazimierczuk, T. Połoński and T. Olszewska, Intermolecular Hydrogen Bonding Directed by Aryl–Perfluoroaryl π–π Stacking Interactions, *Cryst. Growth Des.*, 2023, **23**, 6830–6839.
5 M. Donoshita, Y. Yoshida, M. Hayashi, R. Ikeda, S. Tanaka, Y. Yamamura, K. Saito, S. Kawaguchi, K. Sugimoto and H. Kitagawa, Various Stacking Patterns of Two-Dimensional Molecular Assemblies in Hydrogen-Bonded Cocrystals: Insight into Competitive Intermolecular Interactions and Control of Stacking Patterns, *Angew. Chem. Int. Ed.*, 2021, **60**, 22839–22848.
6 J. R. Palmer, S. B. Tyndall, G. C. Mantel, O. J. Buras, R. M. Young, M. D. Krzyaniak and M. R. Wasielewski, Molecular Cocrystal Packing Suppresses Hopping-Driven Decoherence of Excitonic Spin Qubits, *J. Am. Chem. Soc.*, 2025, **147**, 17394–17403.
7 L. Liu, J.-R. Wang and X. Mei, Enhancing the stability of active pharmaceutical ingredients by the cocrystal strategy, *CrystEngComm*, 2022, **24**, 2002–2022.
8 C. C. Seaton, Building Up Co-Crystals: Structural Motif Consistencies Across Families of Co-Crystals, *Proceedings*, 2020, **78**, 45.
9 C. Aakeröy, Is there any point in making co-crystals?, *Acta Cryst B*, 2015, **71**, 387–391.
10 G. R. Krishna, R. Devarapalli, G. Lal and C. M. Reddy, Mechanically Flexible Organic Crystals Achieved by Introducing Weak Interactions in Structure: Supramolecular Shape Synthons, *J. Am. Chem. Soc.*, 2016, **138**, 13561–13567.
11 S. Hayashi, Elastic Organic Crystals of π-Conjugated Molecules: New Concept for Materials Chemistry, *Symmetry*, 2020, **12**, 2022.

12 P. Bombicz, T. Gruber, C. Fischer, E. Weber and A. Kálmán, Fine tuning of crystal architecture by intermolecular interactions: synthon engineering, *CrystEngComm*, 2014, **16**, 3646–3654.

13 G. Liu, S.-H. Wei and C. Zhang, Review of the Intermolecular Interactions in Energetic Molecular Cocrystals, *Cryst. Growth Des.*, 2020, **20**, 7065–7079.

14 A. J. Cruz-Cabeza, P. R. Spackman and A. V. Hall, The interplay between hydrogen bonds and stacking/T-type interactions in molecular cocrystals, *Commun. Chem.*, 2024, **7**, 284.

15 M. L. Clapham, R. R. Frontiera and C. J. Douglas, Mixed Rubrene Cocrystals Offer Insights into Intermolecular Interactions Influencing Crystal Packing, *Cryst. Growth Des.*, 2023, **23**, 3942–3946.

16 B. Li, L. Liu, Y. Wang, K. Liu, Z. Zheng, S. Sun, Y. Hu, L. Li and C. Li, Structurally diverse macrocycle co-crystals for solid-state luminescence modulation, *Nat. Commun.*, 2024, **15**, 2535.

17 W. Xu, G. Huang, Z. Yang, Z. Deng, C. Zhou, J.-A. Li, M.-D. Li, T. Hu, B. Z. Tang and D. L. Phillips, Nucleic-acid-base photofunctional cocrystal for information security and antimicrobial applications, *Nat. Commun.*, 2024, **15**, 2561.

18 L. Sun, Y. Wang, F. Yang, X. Zhang and W. Hu, Cocrystal Engineering: A Collaborative Strategy toward Functional Materials, *Adv. Mater.*, 2019, **31**, 1902328.

19 T. Wakahara, P. D'Angelo, K. Miyazawa, Y. Nemoto, O. Ito, N. Tanigaki, D. D. C. Bradley and T. D. Anthopoulos, Fullerene/Cobalt Porphyrin Hybrid Nanosheets with Ambipolar Charge Transporting Characteristics, *J. Am. Chem. Soc.*, 2012, **134**, 7204–7206.

20 P. Bhyrappa and K. Karunanithi, Porphyrin−Fullerene, C_{60}, Cocrystallates: Influence of C_{60} on the Porphyrin Ring Conformation, *Inorg. Chem.*, 2010, **49**, 8389–8400.

21 Y. Hao, Y. Wang, L. Spree and F. Liu, Rotation of fullerene molecules in the crystal lattice of fullerene/porphyrin: C_{60} and $Sc_3N@C_{80}$, *Inorg. Chem. Front.*, 2021, **8**, 122–126.

22 P. D. W. Boyd, M. C. Hodgson, C. E. F. Rickard, A. G. Oliver, L. Chaker, P. J. Brothers, R. D. Bolskar, F. S. Tham and C. A. Reed, Selective Supramolecular Porphyrin/Fullerene Interactions1, *J. Am. Chem. Soc.*, 1999, **121**, 10487–10495.

23 T. Ohmura, A. Usuki, Y. Mukae, H. Motegi, S. Kajiya, M. Yamamoto, S. Senda, T. Matsumoto and K. Tatsumi, Supramolecular Porphyrin-Based Metal–Organic Frameworks with Fullerenes: Crystal Structures and Preferential Intercalation of C_{70}, *Chem. Asian J.*, 2016, **11**, 700–704.

24 H. Nobukuni, T. Kamimura, H. Uno, Y. Shimazaki, Y. Naruta and F. Tani, Supramolecular Structures of Inclusion Complexes of C_{70} and Cyclic Porphyrin Dimers, *Bull. Chem. Soc. Jpn.*, 2011, **84**, 1321–1328.

25 Y.-L. Cheng, L. Wei, S.-Z. Liu, X.-G. Yi, W.-T. Chen and W.-S. Lin, A novel supramolecular porphyrin-fullerene compound: Crystal structure and photophysical properties, *J. Solid State Chem.*, 2022, **311**, 123120.

26 T. Wakahara, K. Nagaoka, A. Nakagawa, C. Hirata, Y. Matsushita, K. Miyazawa, O. Ito, Y. Wada, M. Takagi, T. Ishimoto, M. Tachikawa and K. Tsukagoshi, One-Dimensional Fullerene/Porphyrin Cocrystals: Near-Infrared Light Sensing through Component Interactions, *ACS Appl. Mater. Interfaces*, 2020, **12**, 2878–2883.

27 T. Ishii, R. Kanehama, N. Aizawa, M. Yamashita, H. Matsuzaka, K. Sugiura, H. Miyasaka, T. Kodama, K. Kikuchi, I. Ikemoto, H. Tanaka, K. Marumoto and S.-I. Kuroda, Fullerene C_{60} exhibiting a strong intermolecular interaction in a cocrystallite with C_4 symmetrical cobalt tetrakis(di-tert-butylphenyl)porphyrin, *J. Chem. Soc., Dalton Trans.*, 2001, 2975–2980.

28 L. H. Tong, J.-L. Wietor, W. Clegg, P. R. Raithby, S. I. Pascu and J. K. M. Sanders, Supramolecular Assemblies of Tripodal Porphyrin Hosts and C_{60}, *Chem. Eur. J.*, 2008, **14**, 3035–3044.

29 D. V. Konarev, A. L. Litvinov, I. S. Neretin, N. V. Drichko, Y. L. Slovokhotov, R. N. Lyubovskaya, J. A. K. Howard and D. S. Yufit, Formation of Coordination Porphyrin Pentamers in New Supramolecular Complex of Fullerene: $\{(ZnTPP)_4 \cdot 4\text{-}TPyP\} \cdot (C_{60})_2 \cdot (C_6H_5CN)_{3.5}$, *Cryst. Growth Des.*, 2004, **4**, 643–646.

30 M. Roy, I. D. Diaz Morillo, X. B. Carroll, M. M. Olmstead and A. L. Balch, Solvent and Solvate Effects on the Cocrystallization of C_{60} with Co^{II}(OEP) or Zn^{II}(OEP) (OEP = Octaethylporphyrin), *Cryst. Growth Des.*, 2020, **20**, 5596–5609.

31 Y. Wang, H. Wu, W. Zhu, X. Zhang, Z. Liu, Y. Wu, C. Feng, Y. Dang, H. Dong, H. Fu and W. Hu, Cocrystal Engineering: Toward Solution-Processed Near-Infrared 2D Organic Cocrystals for Broadband Photodetection, *Angew. Chem. Int. Ed.,* 2021, **60**, 6344–6350.

32 D. V. Konarev, A. Yu. Kovalevsky, X. Li, I. S. Neretin, A. L. Litvinov, N. V. Drichko, Y. L. Slovokhotov, P. Coppens and R. N. Lyubovskaya, Synthesis and Structure of Multicomponent Crystals of Fullerenes and Metal Tetraarylporphyrins, *Inorg. Chem.*, 2002, **41**, 3638–3646.

33 M. M. Olmstead and D. J. Nurco, Fluorinated Tetraphenylporphyrins as Cocrystallizing Agents for C_{60} and C_{70}, *Cryst. Growth Des.*, 2006, **6**, 109–113.

34 L. M. Baldauf, K. B. Ghiassi, M. M. Olmstead and A. L. Balch, Fullerene nanostructures: how the oblong shape of C_{70} forms a cocrystal with an enormous asymmetric unit and related cocrystals, *Nanoscale*, 2020, **12**, 20356–20363.

35 T. Wakahara, K. Nagaoka, C. Hirata, K. Miyazawa, K. Fujii, Y. Matsushita, O. Ito, M. Takagi, T. Shimazaki, M. Tachikawa, Y. Wada, S. Yagyu, Y. Liu, Y. Nakajima and K. Tsukagoshi, Fullerene C_{70} /porphyrin hybrid nanoarchitectures: single-cocrystal nanoribbons with ambipolar charge transport properties, *RSC Adv.*, 2022, **12**, 19548–19553.

36 E. C. Escudero-Adán, A. Bauzá, L. P. Hernández-Eguía, F. Würthner, P. Ballester and A. Frontera, Solid-state inclusion of C_{60} and C_{70} in a co-polymer induced by metal–ligand coordination of a Zn–porphyrin cage with a bis-pyridyl perylene derivative, *CrystEngComm*, 2017, **19**, 4911–4919.

37 X. Yu, B. Wang, Y. Kim, J. Park, S. Ghosh, B. Dhara, R. D. Mukhopadhyay, J. Koo, I. Kim, S. Kim, I.-C. Hwang, S. Seki, D. M. Guldi, M.-H. Baik and K. Kim, Supramolecular Fullerene Tetramers Concocted with Porphyrin Boxes Enable Efficient Charge Separation and Delocalization, *J. Am. Chem. Soc.*, 2020, **142**, 12596–12601.

38 K. Chida, T. Yoshii, M. Ohwada, Y. Hayasaka, J. Komeda, R. Sakamoto, J. Maruyama, K. Kamiya, M. Inoue, F. Tani and H. Nishihara, Synthesis and electrocatalysis of ordered carbonaceous frameworks from Ni porphyrin with four ethynyl groups, *Catal. Today*, 2023, **411–412**, 113830.

39 T. Yoshii, G. Nishikawa, V. K. Prasad, S. Shimizu, R. Kawaguchi, R. Tang, K. Chida, N. Sato, R. Sakamoto, K. Takatani, D. Moreno-Rodríguez, P. Škorňa, E. Scholtzová, R. K. Szilagyi and H. Nishihara, Quantitative and qualitative analysis of nitrogen species in carbon at the ppm level, *Chem*, 2024, **10**, 2450–2463.

40 N. Sato, R. Toyoda, T. Sato, Z. Lang Goo, S. Takaishi, K. Chida, T. Yoshii, H. Nishihara, K. Sugimoto and R. Sakamoto, Porphyrin/Fullerene Porous Molecular Cocrystal Featuring a

Robust One-Dimensional Channel, *Precis. Chem.*, 2024, **2**, 480–487.

41 X. Yang, M. B. Al-Handawi, L. Li, P. Naumov and H. Zhang, Hybrid and composite materials of organic crystals, *Chem. Sci.*, 2024, **15**, 2684–2696.

42 N. Fukui, T. Kim, D. Kim and A. Osuka, Porphyrin Arch-Tapes: Synthesis, Contorted Structures, and Full Conjugation, *J. Am. Chem. Soc.*, 2017, **139**, 9075–9088.

43 J. Kim, C. Park and H. C. Choi, Selective Growth of a C70 Crystal in a Mixed Solvent System: From Cube to Tube, *Chem. Mater.*, 2015, **27**, 2408–2413.

44 G. B. M. Vaughan, P. A. Heiey, D. E. Luzzi, D. A. Ricketts-Foot, A. R. McGhie, J. E. Fischer, Y.-W. Hui, A. L. Smith, D. E. Cox, W. J. Romanow, B. H. Allen, N. Coustel, J. P. McCauley and A. B. Smith, Orientational Disorder in Solvent-Free Solid C_{70}, *Science*, 1991, **254**, 1350–1353.

45 Y. Sun, X. Wang, B. Yang, M. Chen, Z. Guo, Y. Wang, J. Li, M. Xu, Y. Zhang, H. Sun, J. Dang, J. Fan, J. Li and J. Wei, Trichalcogenasupersumanenes and its concave-convex supramolecular assembly with fullerenes, *Nat. Commun.*, 2023, **14**, 3446.

46 Y. Wang, N. Rinn, K. Eberheim, F. Ziese, J. Christmann, A. Jana, S. Nier, N. W. Rosemann, S. Sanna and S. Dehnen, The π-trap approach for obtaining crystal structure data of inherently amorphous cluster compounds, *Nat. Commun.*, 2025, **16**, 7903.

47 T. D. Kühne, M. Iannuzzi, M. Del Ben, V. V. Rybkin, P. Seewald, F. Stein, T. Laino, R. Z. Khaliullin, O. Schütt, F. Schiffmann, D. Golze, J. Wilhelm, S. Chulkov, M. H. Bani-Hashemian, V. Weber, U. Borštnik, M. Taillefumier, A. S. Jakobovits, A. Lazzaro, H. Pabst, T. Müller, R. Schade, M. Guidon, S. Andermatt, N. Holmberg, G. K. Schenter, A. Hehn, A. Bussy, F. Belleflamme, G. Tabacchi, A. Glöß, M. Lass, I. Bethune, C. J. Mundy, C. Plessl, M. Watkins, J. VandeVondele, M. Krack and J. Hutter, CP2K: An electronic structure and molecular dynamics software package - Quickstep: Efficient and accurate electronic structure calculations, *J. Chem. Phys.*, 2020, **152**, 194103.

48 Y. Xu, S. Zhang, W. Wu and P. Su, Assessments of DFT-based energy decomposition analysis methods for intermolecular interactions, *J. Chem. Phys.*, 2023, **158**, 124116.

49 S. Grimme, Supramolecular Binding Thermodynamics by Dispersion-Corrected Density Functional Theory, *Chem. Eur. J.*, 2012, **18**, 9955–9964.

50 M.-S. Liao, J. D. Watts and M.-J. Huang, Dispersion-corrected DFT calculations on C60-porphyrin complexes, *Phys. Chem. Chem. Phys.*, 2009, **11**, 4365–4374.

51 K. W. Chapman, G. J. Halder and P. J. Chupas, Pressure-Induced Amorphization and Porosity Modification in a Metal−Organic Framework, *J. Am. Chem. Soc.*, 2009, **131**, 17546–17547.

52 B. Yeskendir, J.-P. Dacquin, Y. Lorgouilloux, C. Courtois, S. Royer and J. Dhainaut, From metal–organic framework powders to shaped solids: recent developments and challenges, *Mater. Adv.*, 2021, **2**, 7139–7186.

53 A. Liang, J. Gonzalez-Platas, R. Turnbull, C. Popescu, I. Fernandez-Guillen, R. Abargues, P. P. Boix, L.-T. Shi and D. Errandonea, Reassigning the Pressure-Induced Phase Transitions of Methylammonium Lead Bromide Perovskite, *J. Am. Chem. Soc.*, 2022, **144**, 20099–20108.

54 (*a*) CCDC 2527177: Experimental Crystal Structure Determination, 2026, 10.5517/ccdc.csd.xxxxxxxxxx.
(*b*) CCDC 2527178: Experimental Crystal Structure Determination, 2026, 10.5517/ccdc.csd.xxxxxxxxxx.
(*c*) CCDC 2527179: Experimental Crystal Structure Determination, 2026, 10.5517/ccdc.csd.xxxxxxxxxx.

View Article Online
DOI: 10.1039/D6QI00339G

Journal Name ARTICLE

View Article Online
DOI: 10.1039/D6QI00339G